Angular behavior of the Berreman effect investigated in uniform Al_2O_3 layers formed by atomic layer deposition

Angular behavior of the Berreman effect investigated in uniform Al₂O₃ layers formed by atomic layer deposition

Giovanna Scarel[1], Jeong-Seok Na and Gregory N Parsons

Department of Chemical and Biomolecular Engineering, North Carolina State University,
911 Partners Way, Centennial Campus, Raleigh, NC 27695, USA

E-mail: scarelgx@jmu.edu

Abstract
Experimental transmission absorbance infrared spectra of γ-Al₂O₃ showing evidence of the angular dependence of the peaks of surface modes appearing next to the longitudinal optical phonon frequency ω_{LO} (the Berreman effect) are collected from heat-treated thin oxide films deposited with thickness uniformity on Si(100) using atomic layer deposition. The peak area of the most intense surface longitudinal optical mode is plotted versus the infrared beam incidence angle θ_0. The experimental points closely follow the $\sin^4(\theta_0)$ function in a broad thickness range. The best match occurs at a critical thickness, where a linear relationship exists between the surface longitudinal optical mode intensity and film thickness. Simulations suggest that below the critical thickness the $\sin^4(\theta_0)$ behavior can be explained by refraction phenomena at the air/thin film and thin film/substrate interfaces. Above the critical thickness, the experimentally obtained result is derived from field boundary conditions at the air/thin film interface. The $\sin^4(\theta_0)$ functional trend breaks down far above the critical thickness. This picture indicates that infrared radiation has a limited penetration depth into the oxide film, similarly to electromagnetic waves in conductors. Consequently, surface longitudinal optical modes are viewed as bulk phonons excited down to the penetration depth of the infrared beam. Comparison with simulated data suggests that the infrared radiation absorptance of surface longitudinal optical modes tends to approach the $\sin^2(\theta_0)$ trend. Reflection phenomena are considered to be the origin of the deviation from the $\sin^4(\theta_0)$ trend related to refraction.

(Some figures in this article are in colour only in the electronic version)

1. Introduction

The Berreman effect [1, 2] consists in the increase of surface longitudinal optical (LO) mode [3–10] absorption when infrared (IR) radiation illuminates an oxide film from normal to grazing incidence angle (θ_0) relative to the film surface normal in both transmission [1, 11] and reflection [1] configurations. This pronounced angular dependence of absorption very uniquely characterizes surface LO modes. Therefore, the Berreman effect is exploited as a method to discern the frequencies of LO phonons, to evaluate film dielectric constants [11, 12], to determine crystalline

structures [13–16], and thermal expansion [17]. The sensitivity to system geometry characterizing the Berreman effect in two- (2D) and three-dimensional (3D) structures [18], and the absorption capability of surface LO modes [1, 2, 10], promise possible applications of IR radiation in 3D topography imaging and IR energy harvesting and sensing. For these applications it is important to know the details of the surface LO mode absorption angular behavior in the IR region.

Recently a $\sin^4(\theta_0)$ trend was predicted for surface LO mode absorption in thin oxide films as follows [18]. At the air/thin film interface, kinematic properties [19] of refraction give rise to Snell's law:

$$\frac{[\sin(\theta_0)]}{[\sin(\theta_{film})]} = \frac{n_{film}}{n_{air}}, \qquad (1)$$

---

[1] Author to whom any correspondence should be addressed. Present address: Department of Physics and Astronomy, James Madison University, 901 Carrier Drive, Harrisonburg, VA 22807, USA.

where θ_{film} is the IR beam refraction angle inside the thin film, and n_{film} and n_{air} are the refractive indexes of, respectively, the thin film and air. The relationship between refraction angles at the thin film/substrate interface can be determined in a similar way. For each layer

$$n = \sqrt{\varepsilon}, \qquad (2)$$

where ω is the IR frequency (in cm^{-1}), and ε is the complex dielectric function [20]. It is important that at the frequency of surface LO modes ($\omega = \omega_{\text{LO}}$), an electric field $E_{\perp\text{film}}$ exists inside the ionic oxide thin film, normal to the thin film surface, independent of its interaction with IR radiation [10, 18]. Defining $E_{\perp\text{air}}$ as the IR electric field **E** component outside the thin film and normal to the air/thin film interface, dynamic properties [19], related to the specific nature of the fields involved, determine the boundary conditions of the **E** components normal to the air/thin film interface at $\omega = \omega_{\text{LO}}$ as follows [18, 19]:

$$\frac{\varepsilon_{\text{film}}}{\varepsilon_{\text{air}}} = \frac{E_{\perp\text{air}}}{E_{\perp\text{film}}}, \qquad (3)$$

where $\varepsilon_{\text{film}}$ and ε_{air} are the dielectric functions for, respectively, thin film and air. Combining equation (3) with Snell's law in equation (1), gives

$$\frac{E_{\perp\text{air}}}{E_{\perp\text{film}}} \propto \left| \frac{\sin(\theta_0)}{\sin(\theta_{\text{film}})} \right|^2. \qquad (4)$$

A similar relationship holds at the thin film/substrate interface. Thus, in general, the magnitude $E_{\perp l}$ of the IR beam electric vector **E** normal components at $\omega = \omega_{\text{LO}}$ in each layer, labeled l, of the system (including air) is modulated by refraction phenomena through Snell's law. Assuming that surface LO modes absorb IR energy [1, 2, 10], as opposed to the transverse optical (TO) phonons which reflect IR energy [21], at $\omega = \omega_{\text{LO}}$ it results [18, 22]:

$$A(\omega)_l \propto E_{\perp l}^2, \qquad (5)$$

where $A(\omega)_l$ denotes the absorption in layer l. Combining equation (5) with (4) we obtain

$$A(\omega)_l \propto \sin^4(\theta_l). \qquad (6)$$

The total absorption $A_{\text{tot}}(\omega)$ is the sum of $A(\omega)_l$ over each layer, so that at $\omega = \omega_{\text{LO}}$, $A_{\text{tot}}(\omega)$ is modulated by refractive phenomena in each layer of the sample, and $A_{\text{tot}}(\omega_{\text{LO}}) \propto \sin^4(\theta_0)$. Clarification is needed however on whether the quantity $A_{\text{tot}}(\omega_{\text{LO}})$ corresponds to absorptance [23–25] $\alpha = (1 - T - R) \times 100$, where T is transmittance and R reflectance, or simply to transmission absorbance $-\text{Log}_{10}(T)$. Experimental absorptance in IR spectroscopy requires separate measurement of reflection and transmission, which is cumbersome and rarely adopted for analysis of thin organic and inorganic layers [24–30]. Thus, usually, in transmission IR spectroscopy, simply transmission absorbance is considered.

This work provides an experimental examination of the behavior of the surface LO4 mode transmission absorbance in γ-Al$_2$O$_3$ thin films with increasing IR beam incidence angle θ_0 with respect to sample surface normal. Various
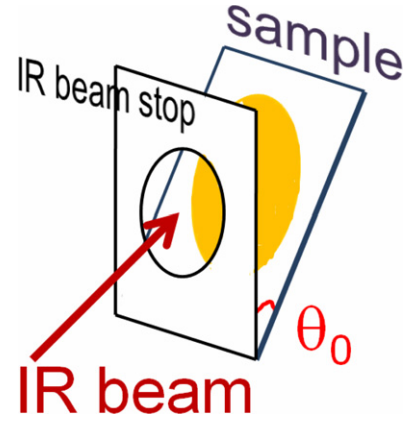

Figure 1. Infrared beam cross section on the surface of γ-Al$_2$O$_3$/Si(100) after the IR beam passes through the beam stop, and forms a θ_0 angle with the normal to the planar γ-Al$_2$O$_3$/Si(100).

simulation methods are used to calculate the angular-dependent behavior of transmission absorbance and absorptance, and simulation results are compared directly with experimental findings. Previous investigations of the angular behavior of surface LO mode transmission absorbance have been undertaken through simulations for the surface LO3 mode of SiO$_2$/Si(100) [31], but models have not been confronted with detailed experimental results. Since features in IR spectra depend on film thickness t [32, 33] and an upper limit exists for the linear relationship between optical phonon absorption and t [11, 34–36], i.e. the critical thickness t_c around 125 nm for γ-Al$_2$O$_3$/Si(100) [36], this work also investigates the $\sin^4(\theta_0)$ functional behavior versus film thickness. Finally, the angular behavior of transmission absorbance $-\text{Log}_{10}(T)$ and absorptance $\alpha = (1 - T - R) \times 100$ of surface LO modes are compared through simulation. An angular dependence study comparing absorbance and absorptance has been undertaken so far only for IR linear dichroism [37].

2. Experimental details

For experimental analyses, Al$_2$O$_3$ films were fabricated by atomic layer deposition (ALD) on Si(100) at 140 °C in a home-made hot wall reactor using alternating pulses of Al(CH$_3$)$_3$, Ar, H$_2$O, and Ar, with duration of 1, 30, 1, and 30 s, respectively [18]. The Si(100) substrate was 1.5×4 cm^2 in area, double-side-polished, n-type doped with 0–100 Ω cm resistivity, showing uniform 60% IR transmittance over the middle infrared (MIR) region (500–4000 cm^{-1}), with the exception of some slight absorption around 630 cm^{-1}. This absorption does not interfere with the surface LO mode of interest for γ-Al$_2$O$_3$. The sample holder for the IR experiments was designed to permit the incident IR beam angle, θ_0, to be readily adjusted, as illustrated in figure 1, to allow the angular dependence of surface LO mode transmission absorbance to be analyzed. The Al$_2$O$_3$ film thickness was measured using ellipsometry (AutoEL, Rudolph Technologies Inc.). The as-grown layers, deposited by applying 300 and 2400 ALD cycles, were, respectively, 35.2 ± 0.2 and 263.0 ± 0.3 nm thick throughout the whole substrate area. Heat treatment in air

Table 1. Assignment, frequencies (in cm^{-1}), and damping factors of γ-Al_2O_3 [42] and SiO_2-related peaks in IR spectra. These parameters are used in IR spectra simulations performed in this work. The value of ε_∞ is 2.91 [42].

Peak	Phonon	Frequency (ω) (cm^{-1})	Damping factor (γ) (cm^{-1})
TO2	TO-γ-Al_2O_3	536	101
TO3	TO-γ-Al_2O_3	744	56
TO4	TO-γ-Al_2O_3	807	43
LO2	LO-γ-Al_2O_3	669	68
LO4	LO-γ-Al_2O_3	917	49
TO-S	TO-SiO_2	1072	—

for 1 h in a furnace at 850 °C promoted crystallization of the amorphous Al_2O_3 layer into γ-Al_2O_3 [18]. The thickness of the heat-treated samples was measured by ellipsometry to be respectively 34.1 ± 0.2 and 247.4 ± 0.2 nm.

Infrared measurements were collected in transmission configuration at incidence angles from $\theta_0 = 0°$ to $81°$ using a Fourier transform IR spectrometer (Nicolet Magna 750). Surface LO modes are excited by the IR radiation electric field component perpendicular to the thin oxide film surface—called the p-component [1, 2, 38–40]. Spectra were acquired with a KBr beamsplitter and a deuterated tri-glycine sulfate (DTGS) detector in the MIR. The typical features of γ-Al_2O_3 are found in the low frequency (ω) range of the MIR. Spectra are plotted in transmission absorbance as $-\mathrm{Log}_{10}(T)$. The magnitude of $-\mathrm{Log}_{10}(T)$ is indicated on each plot. In our experiment, total transmission absorbance is the sum of the contributions of the p- and s-components of IR radiation (the s-component includes the IR radiation electric field component parallel to the thin oxide film surface).

3. Simulation methods

Infrared spectra are simulated for γ-Al_2O_3/Si(100) using a dielectric function $\varepsilon(\omega)_{\mathrm{film}}$ in the zero-and-pole (or factorized) form [41]:

$$\varepsilon(\omega)_{\mathrm{film}} = \varepsilon_\infty \prod_{m=1}^{N} \frac{\omega_{\mathrm{LO}m}^2 - i\omega\gamma_{\mathrm{LO}m} - \omega^2}{\omega_{\mathrm{TO}m}^2 - i\omega\gamma_{\mathrm{TO}m} - \omega^2}. \tag{7}$$

In equation (7) the term i is the imaginary unit and N is the total number of oscillators. The values for surface LO mode and TO phonon frequencies in cm^{-1} (respectively $\omega_{\mathrm{LO}m}$ and $\omega_{\mathrm{TO}m}$), the damping factors ($\gamma_{\mathrm{LO}m}$ and $\gamma_{\mathrm{TO}m}$), and the high frequency value for ε (ε_∞) of γ-Al_2O_3 are as reported by Chu *et al* [42], and are summarized in table 1. Since there are four LO–TO pairs in γ-Al_2O_3, $N = 4$ in our simulations [42]. The dielectric functions for air ($\varepsilon_{\mathrm{air}}$) and Si(100) ($\varepsilon_{\mathrm{Si}}$) are, respectively, $\varepsilon_{\mathrm{air}} = 1$ and $\varepsilon_{\mathrm{Si}} = 4 + i20$ [19]. The constant value chosen for $\varepsilon_{\mathrm{Si}}$ is explained by the uniform 60% IR transmittance found for the used Si(100) substrate in the MIR. The total transmission absorbance is the sum of the contributions to $-\mathrm{Log}_{10}(T)$ of the p- and s-components of IR radiation, as also assumed in the experimental spectra. Absorptance α in % is calculated as $(1 - T - R) \times 100$.

Simulation of the angular behavior of surface LO mode peaks in transmission absorbance and absorptance is pursued by exploiting three different methods to generate IR spectra from the basic parameters (e.g. thickness and dielectric function). The methods used here are referred to as the Hansen [43], the Fuchs, Kliewer and Pardee (or FKP) [44], and the Moreno [31] methods. In each case, the integrated area of a surface LO mode peak is used to evaluate the surface LO mode angular behavior. The simulation methods stem from Maxwell's equations and consider explicitly the finite size of the ionic oxide layer through its thickness t. In addition, thickness t is $t \ll \lambda_{\mathrm{IR}}$, the IR wavelength, so that the interaction between the IR beam and optical phonons takes place within the quasi-static regime. Here, the macroscopic electric field is constant across the oxide film, the solutions of Maxwell's equations coincide with the optical phonons, and polaritons play no significant role [10]. A three-layer system is always considered: the first layer is a transparent medium (air), while the second and third layers (oxide film and Si(100)) can have in general any suitable value of optical constants.

The Hansen method [43] incorporates both kinematic and dynamic properties [19] of reflection and refraction at the air/thin film and thin film/substrate interfaces through Fresnel's formulae applied without approximations to a three-layer system. This approach has been well established to calculate the reflection [38, 45, 46] and transmission [11, 18] of thin multi-layered films exposed to electromagnetic waves. The transmission coefficients T_{p} and R_{p}, affected by phonons excited with the p-component of IR radiation, which contribute to the Berreman effect and in which the dielectric functions are explicit variables [34], are calculated as follows:

$$T_{\mathrm{p}} = \frac{\mathrm{Re}\left(\frac{\xi_{\mathrm{Si}}}{n_{\mathrm{Si}}}\right)}{\cos(\theta_0)/n_{\mathrm{air}}}$$
$$\times \frac{\left|\frac{2\varepsilon_{\mathrm{film}}\xi_{\mathrm{air}}}{\varepsilon_{\mathrm{film}}\xi_{\mathrm{air}}+\varepsilon_{\mathrm{air}}\xi_{\mathrm{film}}}\right|^2 \left|\frac{2\varepsilon_{\mathrm{Si}}\xi_{\mathrm{film}}}{\varepsilon_{\mathrm{Si}}\xi_{\mathrm{film}}+\varepsilon_{\mathrm{film}}\xi_{\mathrm{Si}}}\right|^2 \prod_l e^{-2(2\pi\omega t\xi_l)}}{\left[1 + \left|\frac{\varepsilon_{\mathrm{film}}\xi_{\mathrm{air}}-\varepsilon_{\mathrm{air}}\xi_{\mathrm{film}}}{\varepsilon_{\mathrm{film}}\xi_{\mathrm{air}}+\varepsilon_{\mathrm{air}}\xi_{\mathrm{film}}}\right|\left|\frac{\varepsilon_{\mathrm{Si}}\xi_{\mathrm{film}}-\varepsilon_{\mathrm{film}}\xi_{\mathrm{Si}}}{\varepsilon_{\mathrm{Si}}\xi_{\mathrm{film}}+\varepsilon_{\mathrm{film}}\xi_{\mathrm{Si}}}\right| \prod_l e^{2i(2\pi\omega t\xi_l)}\right]^2} \tag{8a}$$

and

$$R_{\mathrm{p}} = \frac{\left(\frac{\varepsilon_{\mathrm{film}}\xi_{\mathrm{air}}-\varepsilon_{\mathrm{air}}\xi_{\mathrm{film}}}{\varepsilon_{\mathrm{film}}\xi_{\mathrm{air}}+\varepsilon_{\mathrm{air}}\xi_{\mathrm{film}}} + \frac{\varepsilon_{\mathrm{Si}}\xi_{\mathrm{film}}-\varepsilon_{\mathrm{film}}\xi_{\mathrm{Si}}}{\varepsilon_{\mathrm{Si}}\xi_{\mathrm{film}}+\varepsilon_{\mathrm{film}}\xi_{\mathrm{Si}}}e^{2i(2\pi\omega t\xi_l)}\right)^2}{\left[1 + \left|\frac{\varepsilon_{\mathrm{film}}\xi_{\mathrm{air}}-\varepsilon_{\mathrm{air}}\xi_{\mathrm{film}}}{\varepsilon_{\mathrm{film}}\xi_{\mathrm{air}}+\varepsilon_{\mathrm{air}}\xi_{\mathrm{film}}}\right|\left|\frac{\varepsilon_{\mathrm{Si}}\xi_{\mathrm{film}}-\varepsilon_{\mathrm{film}}\xi_{\mathrm{Si}}}{\varepsilon_{\mathrm{Si}}\xi_{\mathrm{film}}+\varepsilon_{\mathrm{film}}\xi_{\mathrm{Si}}}\right| \prod_l e^{2i(2\pi\omega t\xi_l)}\right]^2}. \tag{8b}$$

Here, θ_0 is the incident IR beam angle relative to the oxide surface normal, as illustrated in figure 1, and $\xi_l = n_l \cos(\theta_l)$, where θ_l corresponds to IR beam angle in air, thin film, and substrate (Si(100) in this experiment), as illustrated in the coordinate system reported in [43]. Film thickness t appears explicitly as a parameter in the exponential functions. Defining $\theta_{\mathrm{air}} = \theta_0$, the refraction angles θ_l are obtained through Snell's law as follows:

$$\theta_{\mathrm{film}} = \arcsin\left[\frac{n_{\mathrm{air}}\sin(\theta_0)}{n_{\mathrm{film}}}\right] \tag{9a}$$

$$\theta_{\mathrm{Si}} = \arcsin\left[\frac{n_{\mathrm{film}}\sin(\theta_{\mathrm{film}})}{n_{\mathrm{Si}}}\right]. \tag{9b}$$

The FKP method [44] was originally developed to study optical properties of ionic crystal slabs, which are either

free-standing or assumed on a conductive substrate, and has been extensively used to simulate optical properties, especially reflection, in the IR region [9, 35, 47–49]. The FKP method, in addition to standard field boundary conditions derived from dynamic properties of reflection and refraction [19], includes the effects of retardation of Coulomb forces taking place during coupling between phonons and photons. In the FKP formalism, transmission and reflection coefficients T_p and R_p are calculated as

$$T_p = \frac{1}{4} \left| \frac{1 + \left(\frac{i2\pi\omega\beta}{\gamma_0\varepsilon_{film}}\right)\tan(\pi\omega\beta t)}{1 - \left(\frac{i2\pi\omega\beta}{\gamma_0\varepsilon_{film}}\right)\tan(\pi\omega\beta t)} - \frac{1 - \left(\frac{i2\pi\omega\beta}{\gamma_0\varepsilon_{film}}\right)\cot(\pi\omega\beta t)}{1 + \left(\frac{i2\pi\omega\beta}{\gamma_0\varepsilon_{film}}\right)\cot(\pi\omega\beta t)} \right|^2 \tag{10a}$$

and

$$R_p = \frac{1}{4} \left| \frac{1 + \left(\frac{i2\pi\omega\beta}{\gamma_0\varepsilon_{film}}\right)\tan(\pi\omega\beta t)}{1 - \left(\frac{i2\pi\omega\beta}{\gamma_0\varepsilon_{film}}\right)\tan(\pi\omega\beta t)} + \frac{1 - \left(\frac{i2\pi\omega\beta}{\gamma_0\varepsilon_{film}}\right)\cot(\pi\omega\beta t)}{1 + \left(\frac{i2\pi\omega\beta}{\gamma_0\varepsilon_{film}}\right)\cot(\pi\omega\beta t)} \right|^2. \tag{10b}$$

Here the terms β and γ_0 are defined, respectively, as $\beta = \sqrt{\varepsilon_{film} - \sin^2(\theta)}$ and $\gamma_0 = 2\pi\omega\cos(\theta)$. The coordinate system in the FKP method is reported in [50], where θ is the IR beam angle relative to the oxide slab normal. Here we will examine the FKP method for the case $\theta = \theta_0$, where θ_0 is the IR beam incidence angle with respect to the sample surface normal, as depicted in figure 1 [9, 35, 47–49], and for $\theta = \theta_{film}$, where θ_{film} is as given by Snell's law in equation (9a). In the latter case we label the simulation method as modified FKP. This modification of the FKP formalism is not considered in [44].

Finally, we also consider the method developed by Moreno *et al* [31], based on Fresnel's formulae for multi-layered systems with analytical approximations for transmittance and reflectance of very thin films. In the Moreno method, T_p and R_p are calculated as

$$T_p = \frac{4n_{Si}\cos(\theta_0)}{(\cos(\theta_0) + n_{Si}/\varepsilon_{Si})^2}$$
$$\times \left\{ 1 - \frac{2[\text{Im}(-1/\varepsilon_{film})\sin^2(\theta_0) + \text{Im}(\varepsilon_{film})(n_{Si}/\varepsilon_{Si})\cos(\theta_0)]}{\cos(\theta_0) + n_{Si}/\varepsilon_{Si}} \right.$$
$$\left. \times 2\pi\omega t \right\} \tag{11a}$$

and

$$R_p = \left(\frac{\cos(\theta_0) - n_{Si}/\varepsilon_{Si}}{\cos(\theta_0) - n_{Si}/\varepsilon_{Si}} \right)^2 \left\{ 1 - 4\cos(\theta_0) \right.$$
$$\times \frac{[-\text{Im}(-1/\varepsilon_{film})\sin^2(\theta_0) + (n_{Si}/\varepsilon_{Si})^2\text{Im}(\varepsilon_{film})\cos^2(\theta_0)]}{\cos^2(\theta_0) - (n_{Si}/\varepsilon_{Si})^2 n_{Si}/\varepsilon_{Si}}$$
$$\left. \times 2\pi\omega t \right\} \tag{11b}$$

where θ_0 is defined as the IR beam angle relative to the oxide film normal, as shown in figure 1.

4. Experimental and simulated angular behavior

Experimental IR transmission absorbance $-\text{Log}_{10}(T)$ spectra of a 34.1 nm thick γ-Al$_2$O$_3$/Si(100), obtained with the IR beam incident at $\theta_0 = 0°$, 30°, 60°, and 75° from the sample
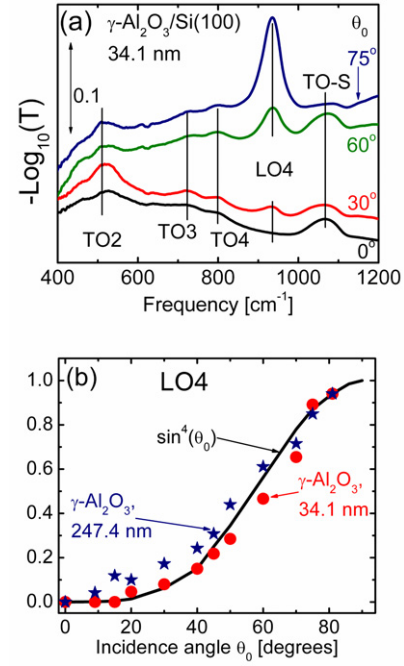

Figure 2. (a) Experimental IR $-\text{Log}_{10}(T)$ spectra (transmission absorbance) at various IR beam incidence angles θ_0 of a 34.1 nm thick γ-Al$_2$O$_3$/Si(100). The TO2, TO3, and TO4 peaks are TO phonons. The LO4 peak is a surface LO mode. The TO-S peak is the TO phonon for the SiO$_2$ layer located between Si(100) and γ-Al$_2$O$_3$. (b) Normalized and corrected LO4 mode experimental integrated peak area (filled circles) from $-\text{Log}_{10}(T)$ spectra versus IR beam incidence angle θ_0 for 34.1 (filled circles) and 247.1 nm (filled stars) thick γ-Al$_2$O$_3$/Si(100) compared to the $\sin^4(\theta_0)$ function (continuous line).

normal, are depicted in figure 2(a). These spectra are similar to those reported in [18] with a multiplication factor. The surface LO mode and TO phonons observed in the sample are labeled, and peak assignments are given in table 1. The surface LO4 mode peak area clearly shows a strong dependence on incidence angle, whereas the area of TO phonons generally shows no angle dependence. The transmission absorbance of the surface LO4 mode peak normalized to the value at $\theta_0 = 81°$ in 34.1±0.2 and 247.4±0.2 nm thick Al$_2$O$_3$/Si(100), collected at various IR beam incident angles, is plotted against angle θ_0 in figure 2(b). The functional form of $\sin^4(\theta_0)$ versus θ_0, which follows the general shape of the experimental results, is also included in the figure. It is noticeable that the experimental points corresponding to the 34.1 nm thick sample concentrate mostly below $\sin^4(\theta_0)$, while those of the 247.4 nm thick γ-Al$_2$O$_3$/Si(100) sample concentrate predominantly above the function.

Infrared transmission absorbance $-\text{Log}_{10}(T)$ spectra simulated using various methods at various IR beam incidence angles θ_0 with respect to the sample surface normal of a 34.1 nm thick γ-Al$_2$O$_3$ film on Si(100) are plotted in figure 3. All spectra exhibit the relevant surface LO modes and TO phonons of γ-Al$_2$O$_3$ (table 1). The surface LO2 mode is clearly visible in spectra generated through the Hansen [43] and the Moreno [31] methods in figures 3(a) and (d). The spectra generated with all methods exhibit an increase in
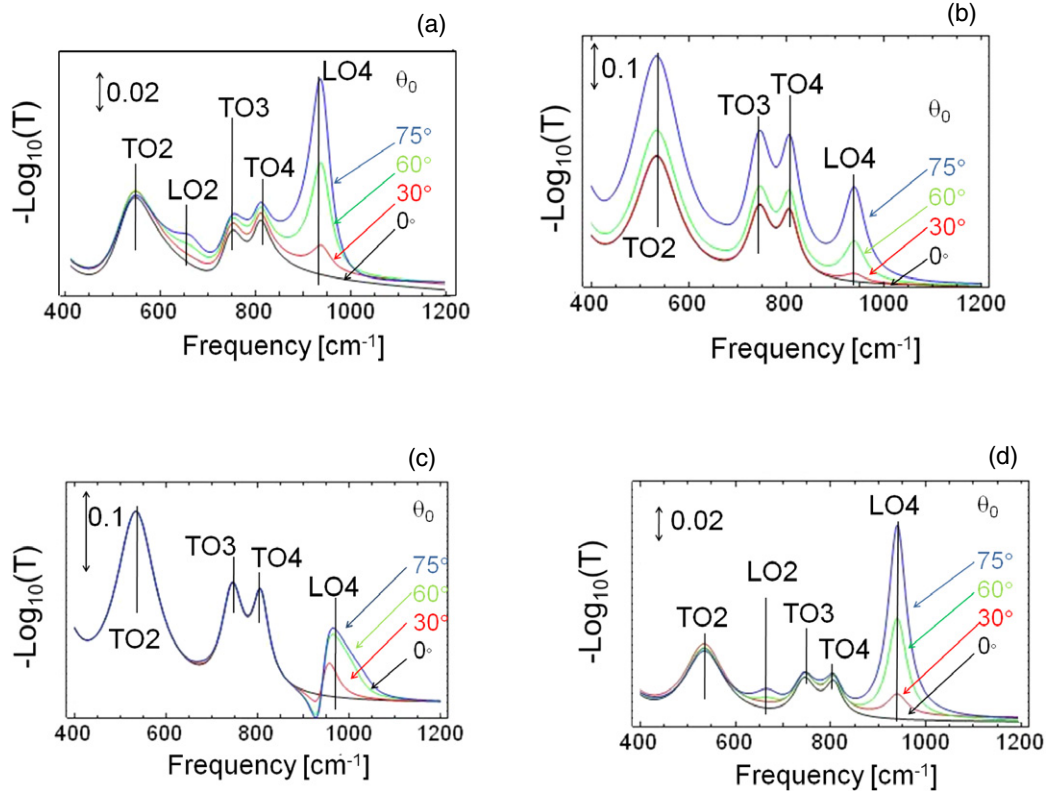
Figure 3. Simulated IR $-\text{Log}_{10}(T)$ spectra (transmission absorbance) at various IR beam incidence angles θ_0 with respect to the sample normal of a 34.1 nm thick γ-Al$_2$O$_3$/Si(100). The TO2, TO3, and TO4 peaks are TO phonons. The LO2 in panels (a) and (d), and LO4 peaks are surface LO modes. The panels depict spectra simulated using, respectively, (a) Hansen [43], (b) FKP [44], (c) modified FKP, and (d) Moreno [31] methods.

the surface LO4 mode peak intensity with increasing IR beam incidence angle θ_0 (Berreman effect) [1, 2], and the height of the surface LO4 mode peak at $\theta_0 = 75°$ is about 0.1, in good agreement with the experimental spectrum in figure 2(a). Moreover, at near grazing incidence angle (75°), the Hansen and the Moreno methods generate spectra that show a surface LO4 mode intensity larger than that of the TO phonon peaks, also consistent with the experimental result in figure 2(a). However, in contrast with the experimental results, the FKP [44] and the modified FKP methods, where $\theta = \theta_0$ and $\theta = \theta_{\text{film}}$ respectively, produce spectra (figures 3(b) and (c)) with a surface LO4 mode peak intensity smaller than the TO phonon peak intensities at all angles modeled.

Figure 4(a) shows the surface LO4 mode peak area in transmission absorbance spectra obtained from the four simulation methods plotted against incidence angle for a 34.1 nm thick γ-Al$_2$O$_3$/Si(100). Figure 4(b) displays the same results with the peak intensity normalized to the value at $\theta_0 = 86°$. For the 34.1 nm thick γ-Al$_2$O$_3$/Si(100), the Hansen [43] and the Moreno [31] methods slightly reproduce the saturation of surface LO4 mode absorbance with increasing angle θ_0. On the other hand, the FKP method [44] generates a surface LO4 mode intensity behavior versus incidence angle θ_0 that increases monotonously. For the modified FKP method the surface LO4 mode intensity versus θ_0 clearly saturates for grazing incidence θ_0 angles, but deviates from the $\sin^4(\theta_0)$ functional trend.

5. Thickness dependence of the $\sin^4(\theta_0)$ trend

Figure 5 illustrates the simulated and normalized surface LO4 mode peak area plotted against incidence angle θ_0 for various values of film thickness from 34 to 248 nm obtained from $-\text{Log}_{10}(T)$ spectra (transmission absorbance) using the Hansen [43] and FKP [44] methods. The γ-Al$_2$O$_3$ film thickness range explored in the simulations spans the critical thickness t_c of 125 nm [36]. Data for the modified FKP and the Moreno methods are not shown and are not further considered: the modified FKP method does not produce spectra exhibiting thickness-dependent variations, whereas the Moreno method produces significant deformations in the spectra, not experimentally observed with increasing oxide film thickness. This behavior is consistent with the thin film approximation incorporated in the Moreno method [31]. According to the Hansen method, the LO4 peak area versus θ_0 follows closely the $\sin^4(\theta_0)$ shape as film thickness approaches t_c (125 nm). Beyond t_c, the simulated points concentrate above the $\sin^4(\theta_0)$ function, in agreement with the experimental results in figure 2(b). Results from the FKP method indicate that, differently from in the case of the 34.1 nm thick film, as film thickness rises toward t_c and beyond, the LO4 peak area approaches the $\sin^4(\theta_0)$ trend except at very grazing angles ($\theta_0 \geqslant 80°$), where reflection features dominate [32]. This behavior is consistent with experimental observations for the 247.4 nm thick sample in figure 2(b). Deviations from the
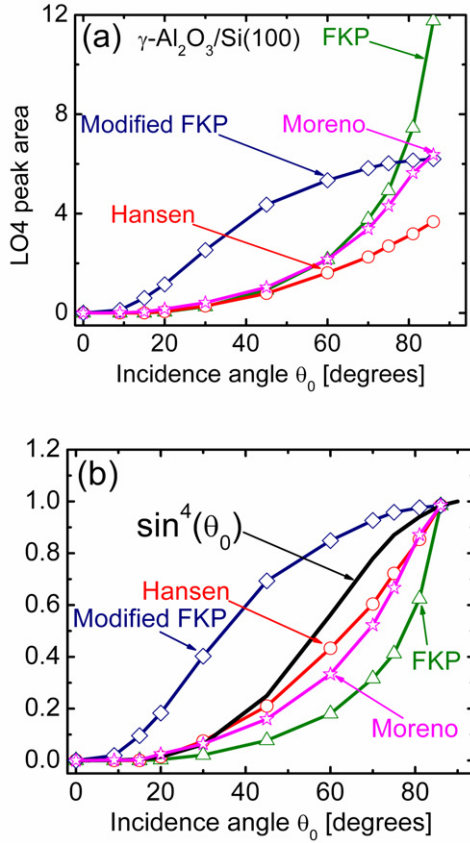
Figure 4. (a) Simulated surface LO4 mode peak area (empty symbols) versus IR beam incidence angle θ_0 for a 34.1 nm thick γ-Al$_2$O$_3$/Si(100) from $-\mathrm{Log}_{10}(T)$ spectra (transmission absorbance). (b) Simulated and normalized surface LO4 mode peak area (empty symbols) from $-\mathrm{Log}_{10}(T)$ spectra versus IR beam incidence angle θ_0 for a 34.1 nm γ-Al$_2$O$_3$/Si(100) compared to the $\sin^4(\theta_0)$ function (continuous line). The simulated data are extracted from spectra generated using Hansen [43], FKP [44], modified FKP, and Moreno [31] methods.

Figure 5. Simulated and normalized surface LO4 mode peak transmission absorbance area (empty symbols) versus IR beam incidence angle θ_0 for γ-Al$_2$O$_3$/Si(100) of variable thickness from 34 to 248 nm. The simulated data are compared to the $\sin^4(\theta_0)$ function (continuous line) and are extracted from $-\mathrm{Log}_{10}(T)$ spectra generated using the (a) Hansen [43], and (b) FKP [44] methods.

$\sin^4(\theta_0)$ trend emerge for films with thickness well above 248 nm. These findings agree with the ability of the FKP method to describe oxide film optical properties in the IR region above t_c [36].

6. Simulated LO4 absorptance versus θ_0 and oxide film thickness

Figure 6 illustrates the simulated LO4 peak intensity in absorptance [23–25] $\alpha = (1 - T - R) \times 100$ spectra versus angle θ_0 obtained for γ-Al$_2$O$_3$/Si(100) in a thickness range from 34 to 248 nm from the Hansen [43] and FKP [44] methods. The corresponding simulated spectra for selected angles are depicted in the insets and are obtained for 125 nm thick γ-Al$_2$O$_3$/Si(100). The modified FKP and the Moreno methods are not considered for the same reasons discussed in section 5. Data obtained from the Hansen method clearly suggest that in absorptance spectra the LO4 peak area versus incidence angle θ_0 generally follows the $\sin^2(\theta_0)$ trend, especially around a critical thickness t_{c2} close to 68 nm. This critical thickness does not correspond to the one defined in the
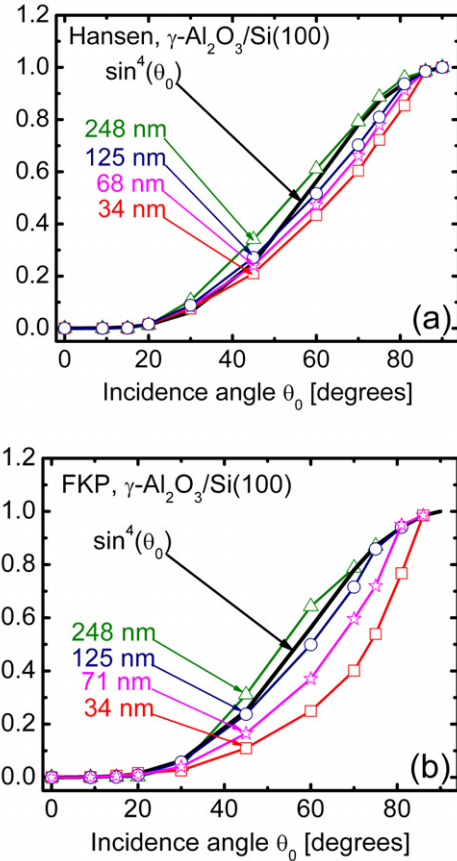
analysis of transmission absorbance. The $\sin^2(\theta_0)$ absorptance trend breaks down toward grazing incidence as oxide thickness increases beyond $\sim t_{c2}$ (68 nm). The very large absorptance of surface LO modes at and below t_c is promising for IR energy harvesting applications. Data for the angular behavior of LO4 from the FKP method also approach the $\sin^2(\theta_0)$ trend in the neighborhood of t_{c2}, especially toward grazing incidence. The trend persists apparently in a broad thickness range above t_{c2}, where the $\sin^2(\theta_0)$ function breaks down at very grazing incidence because reflection phenomena heavily affect the spectra [32]. The decrease in surface LO mode absorptance above t_{c2} is significant, and the absolute value smaller than that of the TO phonons.

7. Role of Snell's law and Fresnel's equation in determining the angular behavior of the Berreman effect

Surface LO modes appear next to ω_{LO} at oblique angles because of the presence of a perpendicular component of the electric field at the thin oxide film surface and in the thin oxide layer [10]. In the Hansen formalism [43], the angular behavior
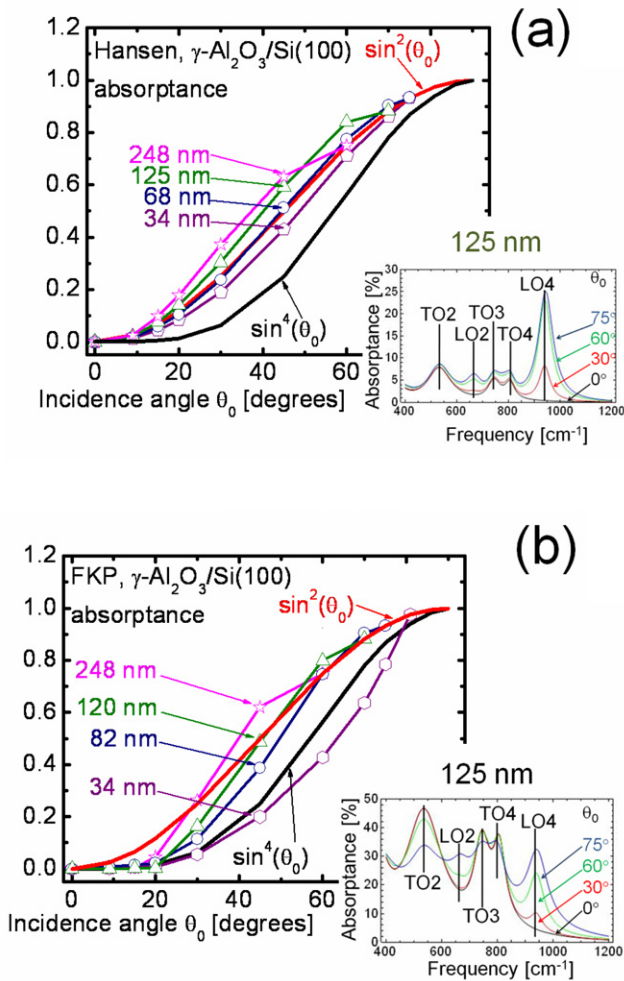
Figure 6. Simulated and normalized surface LO4 mode absorptance area (empty symbols) versus IR beam incidence angle θ_0 for γ-Al$_2$O$_3$/Si(100) of variable thickness from 34 to 248 nm. The simulated absorptance data are compared to the $\sin^2(\theta_0)$ function (continuous line) and are extracted from $(1 - T - R) \times 100$ spectra generated using (a) Hansen [43], and (b) FKP [44] methods. Simulated absorptance spectra at various IR beam incidence angles θ_0 with respect to the sample normal obtained using the Hansen (a) and the FKP (b) methods are shown in the insets for a 125 nm thick γ-Al$_2$O$_3$/Si(100).

of transmission absorbance $-\mathrm{Log}_{10}(T)$ at ω_{LO} is related to the IR beam incidence angle θ_0 and the refractive angles determined through Snell's law (equations (9a) and (9b)). In addition, in the Fresnel's formulae, included in equations (8a) and (8b), reflection and transmission are accounted for in each layer involved in the system. These attributes allow the Hansen method to satisfactorily reproduce the experimental IR spectra in figure 2(a), and the trends of surface LO mode transmission absorbance with incidence angle in figure 2(b) for thin oxide films. On the other hand, in the FKP method [44], the angular behavior of transmission absorbance $-\mathrm{Log}_{10}(T)$ at ω_{LO} is determined at the air/slab interface by θ and by the boundary conditions of the fields involved in the interaction of the IR beam with the examined system [44, 50]. However, these boundary conditions appear not to be sufficient to reproduce the experimental results in figures 2(a) and (b)

for thin oxide films. The presence of the sample substrate is not an issue because the angular trend of surface LO mode transmission absorbance does not depend upon substrate nature [18]. By including Snell's law in the FKP formalism, results in figure 4 show saturation of the surface LO4 mode transmission absorbance versus θ_0, but the trend deviates substantially from the $\sin^4(\theta_0)$ functional behavior. Finally, the Moreno method [31], which also includes approximated Fresnel's formulae, generates spectra in figure 3(d) with good agreement to the experimental spectra in figure 2(a), but not to the $\sin^4(\theta_0)$ trend. This method in addition is limited to film thickness below t_c. The saturation of surface LO mode transmission absorbance with increasing θ_0 is reasonable because a thin film cannot absorb an infinite amount of IR energy as $\theta_0 \rightarrow 90°$. These results for oxide films with thickness $t < t_c$ and $t \ll \lambda_{\mathrm{IR}}$, indicate that understanding the angular dependence of surface LO mode transmission absorbance must include refraction phenomena through Snell's law and the presence of interfaces through Fresnel's formulae. This understanding will extend to all ionic thin film material systems or thin film multi-layers that exhibit the Berreman effect.

8. Limited penetration depth of IR radiation in oxide layers

Observation of figures 5 and 6, focusing on the simulated results from the FKP method, suggests that the sole boundary condition at the air/thin film interface is able to account for the $\sin^4(\theta_0)$ and the $\sin^2(\theta_0)$ trends of surface LO mode transmission absorbance and absorptance versus θ_0 at and above the corresponding critical thicknesses t_c and t_{c2}, respectively, for γ-Al$_2$O$_3$/Si(100). The same figures also suggest that a break-down of the $\sin^4(\theta_0)$ and $\sin^2(\theta_0)$ functional trends takes place far above the critical thicknesses. These observations correlate with the fact that IR radiation penetrates only down to a limited distance from the film surface [36], and indicate that the penetration depth differs depending upon inclusion or non-inclusion of reflection phenomena. The $\sin^4(\theta_0)$ behavior at t_c works for transmission absorbance, in which only refraction is involved, whereas the $\sin^2(\theta_0)$ behavior at t_{2c} works in IR absorption in thin oxide layers where the reflection contribution is included. The critical thicknesses act as a 'skin depth' for IR radiation in insulating oxides, similarly to the skin depth for visible light in metals and conducting oxides [51]. In all these cases, electromagnetic wave transmission decays exponentially as $\mathrm{e}^{-\frac{t}{\delta}}$ with increasing film thickness, where δ is the skin depth for conductors and penetration depth for insulators. Limited penetration depth and exponential attenuation has also been found in the numerical analysis of electromagnetic fields in stratified media [52]. This finding questions the 'surface' nature of surface LO modes [3–10]. These modes appear at the frequencies of LO phonons, which are known for not coupling with photons in bulk crystals [2, 9, 10]. Our results picture surface LO modes as LO phonons coupled to IR photons down to the critical thickness t_c or t_{c2}. This view parallels findings

in other studies that found surface quasi-particles and quasi-particle-related effects to be confined to the first layer from the surface [53]. The context of work by Grechnev *et al* [53] is different compared to ours but it is interesting to notice that, according to these authors, the 'surface' for quasi-particles is truly limited to a very small distance (one atomic layer) from the surface.

9. Possible origin of the split in $\sin^4(\theta_0)$ and $\sin^2(\theta_0)$ trends

Observations of figure 6 suggest that simulated absorptance $\alpha = (1 - T/T_0 - R/R_0) \times 100$ data for the LO4 intensity follow the $\sin^2(\theta_0)$ function in the neighborhood of t_{c2} (on average around 70–75 nm for γ-Al$_2$O$_3$/Si(100)), especially when the simulations are performed with the FKP method. The leading role of reflection phenomena weakens refraction, and determines an absorption expression $A(\omega) \propto E_\perp^2$ as in equation (5) but without a link to Snell's law. Thus, we obtain $A(\omega) \propto E_\perp^2 \propto \sin^2(\theta_0)$. Furthermore, our observations point out that oxide film thickness profoundly modulates the absorption response. The ideal $\sin^4(\theta_0)$ and $\sin^2(\theta_0)$ behaviors hold only at a specific critical distance from the sample surface. The hypothesis is under investigation that this finding correlates with the onset of non-linear behavior in absorptance versus film thickness at a lower thickness than in transmission absorbance. Finally, we observe that reflection phenomena, causing a shift of the LO4 peak, heavily prevail at grazing incidence, where the $\sin^4(\theta_0)$ and $\sin^2(\theta_0)$ trends break down [32]. This result emerges clearly from simulated spectra, but needs more experimental support.

10. Conclusions

We show that the experimentally determined angular behavior of transmission absorbance $-\mathrm{Log}_{10}(T)$ of surface modes located at frequencies next to those of longitudinal optical phonons in a thin oxide film in the infrared region follows the $\sin^4(\theta_0)$ function, where θ_0 is the incidence angle of the infrared beam with respect to the sample normal. The $\sin^4(\theta_0)$ behavior predicted in our estimations is verified experimentally in $-\mathrm{Log}_{10}(T)$ spectra (transmission absorbance) in a thickness range below and in the neighborhood of the critical thickness of 125 nm for γ-Al$_2$O$_3$/Si(100), i.e. the upper thickness limit for a linear relationship between oxide film thickness and phonon transmission absorbance. The $\sin^4(\theta_0)$ trend breaks down far above the critical thickness, and is accurately simulated through Fresnel's equations and Snell's law below the critical thickness, where refraction phenomena dominate. Above the critical thickness, appropriate boundary conditions at the air/thin film interface suffice to account for the experimental results. This finding supports that kinematic and dynamic laws of reflection and refraction are effective in thin films only within a limited distance, equal to the critical thickness, from the air/thin film interface. In this picture, surface longitudinal optical modes act as bulk longitudinal optical phonons excited down to the penetration depth of the infrared beam in thin oxide layers. Simulated data also indicate that, because of the

contribution from reflection, absorptance $\alpha = (1 - T - R) \times 100$ data versus incidence angle for surface longitudinal optical modes satisfy the $\sin^2(\theta_0)$ trend around a critical thickness and slightly beyond. This critical thickness is around 70–75 nm for γ-Al$_2$O$_3$/Si(100). The analysis points out that oxide film thickness profoundly modulates the angular dependence of the absorption response of surface longitudinal optical modes, and that the ideal $\sin^4(\theta_0)$ and $\sin^2(\theta_0)$ behaviors hold only at specific critical distances from the sample surface.

Acknowledgments

References

[1]   Berreman D W 1963 *Phys. Rev.* **130** 2193
[2]   Kittel C 2005 *Introduction to Solid State Physics* (New York: Wiley)
[3]   Ruppin R 1970 *Solid State Commun.* **8** 1129
[4]   Jones W E and Fuchs R 1971 *Phys. Rev.* B **4** 3581
[5]   Chen T S, Alldredge G P and De Wette F W 1972 *Phys. Lett.* A **40** 401
[6]   Ward C A, Alexander R W and Bell R J 1976 *Phys. Rev.* B **14** 856
[7]   Hayashi S, Hirono J, Kanamori H and Ruppin R 1979 *J. Phys. Soc. Japan* **46** 1602
[8]   Frederick B G, Apai G and Rhodin T N 1991 *Phys. Rev.* B **44** 1880
[9]   Vinogradov E A 1992 *Phys. Rep.* **217** 159
[10] Tolstoy V P, Chernyshova I V and Skryshevsky V A 2003 *Handbook on Infrared Spectroscopy of Ultrathin Films* (Hoboken: Wiley)
[11] Bonera E, Scarel G, Fanciulli M, Delugas P and Fiorentini V 2005 *Phys. Rev. Lett.* **94** 027602
[12] Sirenko A A, Bernhard C, Golnik A, Clark A M, Hao J, Si W and Xi X X 2000 *Nature* **404** 373
[13] Hermet P, Goffinet M, Kreisel J and Ghosez P 2007 *Phys. Rev.* B **75** 220102(R)
[14] Scarel G, Debernardi A, Tsoutsou D, Spiga S, Capelli S C, Lamagna L, Volkos S N, Alia M and Fanciulli M 2007 *Appl. Phys. Lett.* **91** 102901
[15] Trasferetti B C, Davanzo C U, Zoppi R A, da Cruz N C and de Moraes M A B 2001 *Phys. Rev.* B **64** 125404
[16] Chambers J J and Parsons G N 2001 *J. Appl. Phys.* **90** 918
[17] Schlesinger Z, Rosen J A, Hancock J N and Ramirez A P 2008 *Phys. Rev. Lett.* **101** 015501
[18] Scarel G, Hyde G K, Hojo D and Parsons G N 2008 *J. Appl. Phys.* **104** 094314
[19] Jackson J D 1999 *Classical Electrodynamics* (New York: Wiley)
[20] Yu P Y and Cardona M 2005 *Fundamentals of Semiconductors. Physics and Materials Properties* (Berlin: Springer)
[21] Ashcroft N W and Mermin N D 1976 *Solid State Physics* (Philadelphia, PA: Saunders)
[22] Angress J F and Maiden A J 1971 *J. Phys. C: Solid State Phys.* **4** 235
[23] Ruppin R 1974 *Phys. Rev.* B **9** 1908
[24] Stierwalt D L, Bernstein J B and Kirk D D 1963 *Appl. Opt.* **2** 1169

[25] Stay B J, Chalmers J M, Mackenzie M W and Mosley D R 1985 *Appl. Spectrosc.* **39** 412
[26] Palik E D, Gibson J W, Holm R T, Hass M, Braunstein M and Garcia B 1978 *Appl. Opt.* **17** 1776
[27] Ohta K and Ishida H 1990 *Appl. Opt.* **29** 2466
[28] Pradhan M M and Arora M 1992 *Opt. Commun.* **94** 428
[29] Cifre J and Roger J P 1998 *Thin Solid Films* **320** 198
[30] Hanssen L 2001 *Appl. Opt.* **40** 3196
[31] Moreno J A, Garrido B, Samitier J and Morante J R 1997 *J. Appl. Phys.* **81** 1933
[32] Gunde M K and Orel Z C 2002 *Appl. Spectrosc.* **56** 24
[33] Gilli E, Horvath A E, Horvath A T, Hirn U and Schennach R 2009 *Cellulose* **16** 825
[34] Harbecke B, Heinz B and Grosse P 1985 *Appl. Phys.* A **38** 263
[35] Scherübl T and Thomas L K 1997 *Appl. Spectrosc.* **51** 844
[36] Scarel G, Na J-S, Gong B and Parsons G N 2010 *Appl. Spectrosc.* **64** 120
[37] Gregoriou V S, Tzavalas S and Bollas S T 2004 *Appl. Spectrosc.* **58** 655
[38] Scarel G, Hirschmugl C J, Yakovlev V V, Sorbello R S, Aita C R, Tanaka H and Hisano K 2002 *J. Appl. Phys.* **91** 1118

[39] Yamamoto K and Ishida H 1995 *Appl. Opt.* **34** 4177
[40] Yamamoto K and Ishida H 1994 *Vib. Spectrosc.* **8** 1
[41] Berreman D W and Unterwald F C 1968 *Phys. Rev.* **174** 791
[42] Chu Y T, Bates J B, White C W and Farlow G C 1988 *J. Appl. Phys.* **64** 3727
[43] Hansen W N 1968 *J. Opt. Soc. Am.* **58** 380
[44] Fuchs R, Kliewer K L and Pardee W J 1966 *Phys. Rev.* **150** 589
[45] Rivnay J, Jimison L, Toney M F, Preiner M, Melosh N A and Salleo A 2008 *J. Vac. Sci. Technol.* B **26** 1454
[46] Shan X, Foley K J and Tao N 2008 *Appl. Phys. Lett.* **92** 133901
[47] Scarel G, Aita C R and Sklyarov A V 2003 *J. Non-Cryst. Solids* **318** 168
[48] Mochizuki S 1989 *J. Phys.: Condens. Matter* **1** 10351
[49] Hisano K and Toda K 1982 *J. Phys. C: Solid State Phys.* **15** 1111
[50] Kliewer K L and Fuchs R 1966 *Phys. Rev.* **150** 573
[51] Porch A, Morgan D V, Perks R M, Jones M O and Edwards P E 2004 *J. Appl. Phys.* **95** 4734
[52] Li K 2009 *Electromagnetic Fields in Stratified Media* (Berlin: Springer)
[53] Grechnev A, Di Marco I, Katsnelson M I, Lichtenstein A I, Wills I and Eriksson O 2007 *Phys. Rev.* B **76** 035107